To appear in the Astrophysical Journal, 572, 2002 June
Preprint typeset using LaTeX style emulateapj v. 19/02/01

AN X-RAY REPROCESSING MODEL OF DISK THERMAL EMISSION IN TYPE 1 SEYFERT GALAXIES

James Chiang[1]
NASA/GSFC, Code 661, Greenbelt MD 20771
To appear in the Astrophysical Journal, 572, 2002 June

ABSTRACT

Using a geometry consisting of a hot central Comptonizing plasma surrounded by a thin accretion disk, we model the optical through hard X-ray spectral energy distributions of the type 1 Seyfert galaxies NGC 3516 and NGC 7469. As in the model proposed by Poutanen, Krolik, & Ryde for the X-ray binary Cygnus X-1 and later applied to Seyfert galaxies by Zdziarski, Lubiński, & Smith, feedback between the radiation reprocessed by the disk and the thermal Comptonization emission from the hot central plasma plays a pivotal role in determining the X-ray spectrum, and as we show, the optical and ultraviolet spectra as well. Seemingly uncorrelated optical/UV and X-ray light curves, similar to those which have been observed from these objects can, in principle, be explained by variations in the size, shape, and temperature of the Comptonizing plasma. Furthermore, by positing a disk mass accretion rate which satisfies a condition for global energy balance between the thermal Comptonization luminosity and the power available from accretion, one can predict the spectral properties of the heretofore poorly measured hard X-ray continuum above $\sim 50\,\mathrm{keV}$ in type 1 Seyfert galaxies. Conversely, forthcoming measurements of the hard X-ray continuum by more sensitive hard X-ray and soft γ-ray telescopes, such as those aboard the *International Gamma-Ray Astrophysics Laboratory* (*INTEGRAL*) in conjunction with simultaneous optical, UV, and soft X-ray monitoring, will allow the mass accretion rates to be directly constrained for these sources in the context of this model.

Subject headings: galaxies: active — galaxies: individual (NGC 3516, NGC 7469) — galaxies: Seyfert — X-rays: galaxies

1. INTRODUCTION

An important characteristic of type 1 Seyfert galaxies (hereafter Seyfert 1s) is the highly correlated variability of the continuum flux across a wide range of optical and ultraviolet wavelengths. The short relative lags between the various bands and the observed optical/UV color variations have been interpreted as evidence of thermal reprocessing by the accretion disk of higher energy emission from a single, relatively compact source (Krolik et al. 1991; Courvoisier & Clavel 1991; Collin-Souffrin 1991). The principal candidate for this emission is the power-law-like X-ray continuum which is believed to be produced via thermal Comptonization in regions of hot plasma near the central black hole. Observations of relativistically broadened iron Kα emission lines and the so-called Compton reflection hump provide further evidence that a substantial amount of X-ray flux is intercepted and reprocessed by a thin accretion disk in these systems.

Recent multiwaveband monitoring observations of Seyfert 1s have shown that the optical/UV emission is not related to the observed X-ray flux in any simple way. In June–July 1996, a ~ 30 day UV and X-ray monitoring campaign of NGC 7469 by the *International Ultraviolet Explorer (IUE)* and the *Rossi X-ray Timing Experiment (RXTE)* showed that although the UV and 2–10 keV X-ray light curves displayed some rough similarities in variability amplitudes and time scales, they were not related in a fashion that would naively be expected from thermal reprocessing (Nandra et al. 1998). In particular, the UV maxima preceded similar features in the X-rays by ~ 4 days, while the minima in both light curves occurred nearly simultaneously. A more recent analysis of these data revealed, however, that the UV light curve is well correlated with the X-ray spectral index as well as with the extrapolated X-ray flux in the 0.1–100 keV band. This suggests that there is a causal connection between the X-ray and UV emission in this object (Nandra et al. 2000). In April 1998, an intensive 3-day optical/UV/X-ray monitoring observation of NGC 3516 by the *Hubble Space Telescope (HST)* and *RXTE* showed optical fluxes which changed only by $\sim 3\%$ (peak-to-peak) while the 2–10 keV X-ray flux varied by $\sim 60\%$. Furthermore, the shapes of the variations in the optical and X-ray light curves were only marginally similar. Nonetheless, the variability at optical wavelengths, from 3590 Å to 5510 Å, was highly correlated with essentially zero lag between the different continuum bands, consistent with the thermal reprocessing model (Edelson et al. 2000).

Chiang & Blaes (2001a; hereafter Paper I) have shown that the 1998 optical and X-ray observations of NGC 3516 can largely be explained by a thermal Comptonization/disk reprocessing model similar to that proposed by Poutanen, Krolik, & Ryde (1997) to account for the differences between the hard and soft spectral states in the Galactic X-ray binary Cygnus X-1. This model was also applied in a simplified form by Zdziarski, Lubiński, & Smith (1999; hereafter ZLS) to both X-ray binaries and Seyfert galaxies in order to explain an apparent correlation between the X-ray spectral index and the relative magnitude of the Compton reflection component. In Paper I, we found that inversely-related changes in the size and X-ray luminosity of the Comptonizing plasma can produce the relatively large variations in the 2–10 keV band while causing only much smaller variations in the disk thermal reprocessed emission. With the addition of disk emission due to internal viscous dissipation, we found that the optical and X-ray variations could be roughly matched while simultaneously satisfying an energy balance condition relating the bolometric luminosity to the radiative power available through disk accretion.

[1] Also at Joint Center for Astrophysics/Physics Department, University of Maryland, Baltimore County, Baltimore MD 21250

In this paper, we refine the calculations for NGC 3516 presented in Paper I by explicitly fitting the optical and X-ray continuum data and producing broad band spectral energy distributions (SEDs) for each observing epoch. In addition, we apply these calculations to the 1996 UV/X-ray monitoring observations of NGC 7469 in order to provide a more complete physical picture for the correlations found by Nandra et al. (2000). We proceed by discussing the relevant optical, UV, and X-ray observations in §2. In §3, we describe the thermal Comptonization and disk reprocessing model including our modifications of the geometry of the Comptonizing region and empirical color corrections for the disk emission. The results for NGC 3516 and NGC 7469 are presented in §4; and we discuss these results and conclude in §5.

2. OBSERVATIONS

For the 2–10 keV fluxes and spectral indices of NGC 3516, we have fit the archival *RXTE/Proportional Counter Array (PCA)* data for the April 1998 observations. Our X-ray spectral model consisted of an exponentially cut-off power-law plus a Compton reflection component (the PEXRAV model in XSPEC v10.0), a Gaussian line for the Fe Kα emission line and neutral absorption for the foreground column density. The cut-off energy for the exponential roll-over was set at $E_c = 120$ keV which is sufficiently high so that it does not affect the inferred power-law index in the 2–10 keV band. We find somewhat softer spectral indices than Nandra et al. (1999) who analyzed the simultaneous observations by the *Advanced Satellite for Cosmology and Astrophysics (ASCA)*. This discrepancy is due to the fact that these authors did not include a Compton reflection component in their analysis (K. Nandra 2001, private communication). The optical continuum variations have been taken from Fig. 2 of Edelson et al. (2000), and the mean optical fluxes at 5510 Å, 4235 Å, and 3590 Å are from their Table 1.[2] Because of the small aperture of the *HST/Space Telescope Imaging Spectrograph*, we do not apply a starlight correction. We do make an extinction correction using E(B–V) = 0.042 (Schlegel, Finkbeiner, & Davis 1998) and the reddening law of Cardelli et al. (1989). The flux measurements at 1360 Å made by Edelson et al. were not simultaneous with the optical data, and as these authors discuss, the UV measurements are affected by detector gain changes induced by thermal variations. Therefore, we restrict our analysis of the disk thermal emission to the optical bands. Since spectral fitting of the X-ray data entailed integration times of $\sim$ 30–70 ks (see Table A1), the optical fluxes used in the SED fits were averaged over the duration of each of these epochs. If the optical emission is due to disk reprocessing, it is expected to be produced at relatively large distances ($r > 10^{14}$ cm) from the central black hole. In accord with this, we have shifted the optical light curves by the measured peak lag of −0.21 days relative to the 2–10 X-ray light curve (Edelson et al. 2000). The times of each observing epoch, the X-ray fit parameters, and the corrected and time-shifted optical fluxes are given in Table A1.

The optical and UV continuum fluxes for NGC 7469 were obtained from the AGN Watch web page (`http://astronomy.ohio-state.edu/~agnwatch/`). We use the 4865 Å and 6962 Å continuum light curves measured by Collier et al. (1998) and the modified 1315 Å light curves of Kriss et al. (2000). Welsh et al. (1998) compared the ground-based optical spectra of Collier et al. to contemporaneous *HST* spectra and found that the ground-based spectra are substantially redder due to contamination from starburst activity in the host galaxy. In order to determine the continuum emission due to the Seyfert nucleus, we used the difference between the *HST* and the mean ground-based spectra to estimate the starlight contribution. The simultaneous UV data were obtained using *IUE* (Wanders et al. 1997; Kriss et al. 2000), and Welsh et al. (1998) showed that the *IUE* and *HST* fluxes at 1315 Å were consistent over a half-day period during the 30-day monitoring campaign. Thus, despite the relatively large aperture used for the *IUE* spectra, we assume that the starlight contribution to be negligible at this wavelength. A reddening correction using E(B–V) = 0.12 has been applied to the optical and UV fluxes. This correction includes a Galactic component as well as absorption intrinsic to NGC 7469 (Kriss et al. 2000). The mean corrected optical and UV fluxes are $F_{1315} = 11.4$, $F_{4865} = 1.59$, and $F_{6962} = 0.75$, all in units of 10^{-14}erg cm^{-2}s^{-1}Å^{-1}. The X-ray fluxes and spectral indices are taken from Nandra et al. (2000) who fit the *RXTE/PCA* data with the same model we used for NGC 3516. The optical and UV fluxes have been linearly interpolated from the AGN Watch data at the observing times of the X-ray data. The fluxes at 4865 Å and 6962 Å were time-shifted by the measured lags relative to the 1315 Å light curve: −1.0 days for the 4865 Å data and −1.5 days for the 6962 Å data (Collier et al. 1998).

3. THE MODEL: THERMAL COMPTONIZATION GEOMETRY, ENERGY BALANCE, AND THE DISK SPECTRUM

The geometry we consider is similar to that proposed by Shapiro, Lightman, & Eardley (1976) in their two-temperature disk model of Cygnus X-1: a central, geometrically thick region of hot plasma surrounded by a relatively cold, thin accretion disk. In principle, the hot central region could arise because of a thermal instability as originally envisioned by Shapiro et al. (1976), or it could consist of an advection dominated accretion flow (ADAF) (e.g., Narayan & Yi 1995) or any one of its more recent variations (Blandford & Begelman 1999; Narayan, Igumenshchev, & Abramowicz 2000; Quataert & Gruzinov 2000). Following Poutanen et al. (1997), our goal is to infer the properties of the disk and Comptonizing plasma from the radiation physics and thereby provide constraints for the dynamical models of the inner accretion flow which may help distinguish between the various candidates.

A key feature of the present calculations is the thermostatic feedback effect between the X-ray emission from the Comptonizing plasma and the soft photons which are produced by thermal reprocessing of these X-rays by the accretion disk (Haardt & Maraschi 1991; Stern et al. 1995). ZLS noted that the degree of feedback can be adjusted by altering the geometry of the hot plasma, and they invoked this mechanism to explain the apparent correlation between the X-ray spectral index, Γ, and the relative magnitude, R, of the Compton reflection component in Seyfert galaxies and X-ray binaries. Following Poutanen et al. 1997 and similar results Zdziarski et al. (1998) obtained by applying a similar analysis to the X-ray binary GX339–4, ZLS proposed that the region of Comptonizing plasma takes the form of a uniform, optically thin sphere centered on the black hole. The X-ray spectral index variations occur because the disk penetrates the plasma sphere by different

[2] For the spectral fitting, optical and UV wavelengths have been de-redshifted to the source rest frame using $z = 0.0088$ and $z = 0.0163$ for NGC 3516 and NGC 7469, respectively.

amounts due to changes in the sphere radius, r_s, and/or changes in the disk inner truncation radius, $r_{\rm min}$. Greater overlap of the disk by the sphere results in a larger fraction of the X-ray emission being intercepted by the disk and also in a larger amount of reprocessed flux. This produces an increased Compton reflection component as well as more soft disk photons entering the hot plasma. The additional disk flux provides enhanced cooling of the plasma by increasing Compton losses; and the equilibrium temperature of the plasma decreases, thus producing a softer X-ray spectrum. Using estimates for the fraction of thermally reprocessed emission intercepted by the plasma sphere as a function of the ratio $r_{\rm min}/r_s$ and an empirical relationship between the Compton amplification factor, A, and the spectral index of the thermal Comptonization continuum (Beloborodov 1999),

$$\Gamma = 2.33(A-1)^{-1/10}, \tag{1}$$

ZLS derived an R-Γ relation which is similar to the observed correlation found in the X-ray spectra of Seyfert 1s.

The radial distribution of the flux incident upon a razor-thin disk due to isotropic emission from an optically thin sphere is given by

$$F_{\rm inc}(r) = \frac{3}{16\pi^2}\frac{L_x}{r_s^2}h\left(\frac{r}{r_s}\right), \tag{2}$$

where L_x is the total thermal Comptonization luminosity. The dimensionless function $h(r/r_s)$ is Eq. 1 of ZLS. It has the asymptotic behavior $h(r/r_s \gg 1) \rightarrow (\pi/4)(r_s/r)^3$ and is approximately flat for $r/r_s \lesssim 1$ with $h(0) = \pi$. In Paper I, we calculated the disk thermal spectrum by assuming local blackbody emission and estimated the local disk temperature as being due to a combination of reprocessed flux and emission due to internal viscous dissipation:

$$T_{\rm disk}(r) = \left[\frac{(1-a)F_{\rm inc}(r)+F_{\rm visc}(r)}{\sigma_B}\right]^{1/4}, \tag{3}$$

where $a = 0.15$ is the assumed disk albedo and σ_B is the Stefan-Boltzmann constant. As in Paper I, here we model the flux due to viscous dissipation as

$$F_{\rm visc}(r) = \frac{3}{8\pi}\frac{GM\dot{M}}{r^3}\left[1-\left(\frac{r_I}{r}\right)^{1/2}\right], \tag{4}$$

where M is the black hole mass, $\dot{M}$ is the mass accretion rate, and r_I is the "effective" disk inner radius which we hereafter take to be $r_I = r_g \equiv GM/c^2$, appropriate for a maximal Kerr metric.

In Paper I, we showed that the near constant optical continuum of NGC 3516 in the presence of large variations in the X-ray flux could be explained in this model if the thermal Comptonization luminosity were inversely proportional to the radius of the plasma sphere, $L_x \propto r_s^{-1}$. In addition, we found that the disk inner truncation radius had to be fairly constant on time scales longer than the 3-day observation in order to avoid excessive color variations in the optical and UV bands. However, if one assumes that the contribution to the disk thermal emission from internal viscous dissipation is negligible, then the amount of X-ray luminosity required to produce the observed optical continuum levels result in 2–10 keV fluxes which exceed the observed values by a factor ~ 4. The addition of viscous dissipation in the disk can reduce the needed X-ray luminosity substantially; and as it turns out, the amount of viscous dissipation required to reproduce the mean X-ray spectrum also satisfies an energy balance condition:

$$L_{\rm untr} \approx L_x + L_{\rm disk} \tag{5}$$

where $L_{\rm disk}$ is the luminosity of the disk thermal emission due to viscous dissipation assuming that the inner disk is cut-off at the truncation radius $r_{\rm min}$, and $L_{\rm untr}$ is the total luminosity from viscous dissipation for an untruncated thin disk extending all the way down to r_I:

$$L_{\rm disk,untr} = 4\pi\int_{r_{\rm min},r_I}^{\infty} r\,dr\,F_{\rm visc}(r). \tag{6}$$

The difference $L_{\rm untr} - L_{\rm disk}$ can be interpreted as the accretion power that would otherwise emerge as local blackbody emission from the inner regions of the disk that is instead being used to heat the Comptonizing plasma.

If one neglects local viscous dissipation, the intercepted seed photon luminosity is given by $L_s = L_x\tilde{L}_s$, where $\tilde{L}_s$ is a function only of the quantity $r_{\rm min}/r_s$ (ZLS). Since the Compton amplification factor is the ratio of the thermal Comptonization luminosity and the seed photon luminosity, $A \equiv L_x/L_s = 1/\tilde{L}_s$, it too is a function only of $r_{\rm min}/r_s$. In particular, its value monotonically decreases as $r_{\rm min}/r_s$ increases. For $r_{\rm min}/r_s = 1$ and using Eq. 1, the equilibrium photon index is $\Gamma = 1.55$. Since the fitted X-ray spectral indices for NGC 3516 are $\Gamma \sim 1.65$, this implies that the plasma sphere must overlap disk so that $r_s > r_{\rm min}$ for this model, assuming zero viscous dissipation.

The inclusion of viscous dissipation has two effects on the amplification factor. First, as we note above, it reduces the X-ray luminosity required to produce the observed optical emission. Second, it acts as a constant offset to the ZLS value of L_s. Both of these effects reduce the amplification factor for a given ratio $r_{\rm min}/r_s$ and cause the associated X-ray spectral index to be larger (Eq. 1). For fits to the NGC 3516 data presented in Paper I, the viscous dissipation needed to fit the X-ray fluxes was large enough to require that the radius of the Comptonizing sphere had to be smaller than the disk inner radius. In the context of the plasma sphere geometry, this implies a large gap between the hot plasma and the inner edge of the thin disk. In order to avoid such a gap, we have modified the shape of the central hot plasma for cases where smaller disk covering factors (i.e., smaller values of spectral index) are required. For $r_s < r_{\rm min}$, we take the shape of the Comptonizing plasma to be an oblate ellipsoid with the variable r_s denoting its semi-minor axis. For $r_s \geq r_{\rm min}$, the Comptonizing region is spherical as before. Figure A1 illustrates these two cases.

For $r_s \geq r_{\rm min}$, the radial distribution of thermal Comptonized flux incident upon the disk is given by Eq. 2. For $r_s < r_{\rm min}$, it is

$$F_{\rm inc}(r) = \frac{3L_x}{16\pi^2 {r_{\rm min}}^2 r_s}\int_0^{\alpha_{\rm max}}\sin\alpha\cos\alpha\,d\alpha\int_{-\phi_{\rm max}}^{\phi_{\rm max}} l\,d\phi, \tag{7}$$

where α is the angle an incoming ray makes with the disk plane, ϕ is its azimuthal angle, and $l = l(r,\alpha,\phi;r_s)$ is the path length through the Comptonizing region (see Fig. A1). Explicit formulae for l, $\alpha_{\rm max}$, and $\phi_{\rm max}$ are given in the Appendix.

The seed photon luminosity for the Comptonization process is the disk flux which enters the region of hot plasma. For our geometry, this is given by

$$L_s = 4\pi\int_{r_{\rm min}}^{\infty} g(\tilde{r})\,I(r)\,r\,dr, \tag{8}$$

where $I(r) = [(1-a)F_{\rm inc} + F_{\rm visc}]/\pi$ is the disk surface brightness, $\tilde{r} = r/r_{\rm min}$, and we have defined

$$g(\tilde{r}) = 2\int_0^{\alpha_{\rm max}}\phi_{\rm max}(\alpha,\tilde{r})\sin\alpha\cos\alpha\,d\alpha. \tag{9}$$

In Fig. A2, we plot the ratio of the seed photon luminosity to X-ray luminosity, L_s/L_x, as a function of $r_s/r_{\rm min}$ for the case where the disk emission is due entirely to thermal reprocessing. For comparison, we plot the results for the sphere+disk model described by ZLS and the hybrid sphere/ellipsoid model.

We include an empirical color correction for the disk thermal emission as a function of radius. Hubeny et al. (2000, 2001) have modeled disk atmospheres appropriate for Seyfert nuclei and find that the optical continuum can be moderately well approximated by local blackbody emission, but at UV wavelengths and higher, significant deviations occur. This also seems to be true for disks powered solely by external illumination (Sincell & Krolik 1997). Since we are modeling the UV emission for NGC 7469, a color correction, in principle, should be applied. We adopt a temperature dependent color correction of the form

$$f_{\rm col}(T_{\rm disk}) = f_\infty - \frac{(f_\infty - 1)(1+\exp(-\nu_b/\Delta\nu))}{1+\exp((\nu_p-\nu_b)/\Delta\nu)}, \qquad (10)$$

where $\nu_p \equiv 2.82 k_B T_{\rm disk}/h$ is the peak frequency of a blackbody with temperature $T_{\rm disk}$. This expression for $f_{\rm col}$ goes from unity at low temperatures to f_∞ at high temperatures with a transition at $\nu_b \approx \nu_p$. We find that $f_\infty = 2.3$ and $\nu_b = \Delta\nu = 5\times10^{15}$ Hz do a reasonable job of reproducing the model disk spectra of Hubeny et al. (2001).

We fit the observed optical, UV and X-ray data in the following manner: For a given trial value of plasma temperature, T, the thermal Comptonization continuum is modeled as an exponentially cut-off power-law:

$$L_E = (L_0/E_c)(E/E_c)^{1-\Gamma}\exp(-E/E_c), \qquad (11)$$

where we set $E_c = 2k_BT$ appropriate for plasma Thomson depths $\tau \lesssim 1$. The normalization L_0 is given by

$$F_{2\text{-}10} = \frac{L_0}{4\pi d_l^2}\int_{2\,{\rm keV}/E_c}^{10\,{\rm keV}/E_c}\left(\frac{E}{E_c}\right)^{1-\Gamma}\exp(-E/E_c)d(E/E_c), \qquad (12)$$

where $F_{2\text{-}10}$ is the measured 2–10 keV flux and d_l is the luminosity distance to the source. The total thermal Comptonization luminosity is then

$$L_x = L_0\int_{E_{\rm min}/E_c}^{\infty}\left(\frac{E}{E_c}\right)^{1-\Gamma}\exp(-E/E_c)d(E/E_c), \qquad (13)$$

where we have set the minimum photon energy at a nominal value of $E_{\rm min} = 0.01$ keV.

Having determined the thermal Comptonization luminosity for a given plasma temperature, we find the value of r_s which provides the best-fit disk spectrum:

$$F_\nu = \frac{4\pi\cos i}{d_l^2}\frac{h\nu^3}{c^2 f_{\rm col}^4}\int_{r_{\rm min}}^{\infty}\frac{r\,dr}{\exp(h\nu/f_{\rm col}k_BT_{\rm disk})-1}, \qquad (14)$$

where i is the observer inclination, and the disk temperature is given by Eq. 3. We then use the best-fit value of r_s to compute the corresponding seed photon luminosity, L_s, the Compton amplification factor $A = L_x/L_s$, and the *predicted* value of the X-ray photon spectral index, $\Gamma_{\rm model}$. In contrast to ZLS and Paper I, we use the relation

$$\Gamma_{\rm model} = 2.15(A-1)^{-1/14} \qquad (15)$$

rather than Eq. 1 of Beloborodov (1999). Malzac, Beloborodov, & Poutanen (2001) obtained this parameterization for pill-box shaped coronae atop an accretion disk using a Monte Carlo method to compute the thermal Comptonization continuum, and we have found a nearly identical relation from our own Monte Carlo simulations of thermal Comptonization and disk thermal reprocessing in the sphere+disk geometry (Chiang & Blaes 2001b). The best-fit value of the plasma temperature T has been ascertained when the predicted photon spectral index matches the measured spectral index. The effective Thomson depth, $\tau_{\rm eff}$, of the Comptonizing plasma is estimated by inverting another empirical relation found by Beloborodov (1999),

$$\Gamma = \frac{9}{4}y^{-2/9}, \qquad (16)$$

where the Compton y-parameter is $y \equiv 4\theta_e(1+4\theta_e)\tau_{\rm eff}(1+\tau_{\rm eff})$ and $\theta_e \equiv k_BT/m_ec^2$. Although the specific values of $\tau_{\rm eff}$ that we find have no substantive role in our calculations, they may provide, along with the plasma temperatures, useful constraints on the properties of the Comptonizing region for the dynamical models.

The other important model parameters are the disk inner truncation radius, $r_{\rm min}$, the central black hole mass, M, and the mass accretion rate, $\dot{M}$. We assume that these quantities are constant throughout the monitoring campaigns for each object. The black hole masses can certainly be taken to be constant, and $r_{\rm min}$ and $\dot{M}$ will likely only change appreciably on viscous time scales which are on the order of $\mathcal{O}(10^1)$ years for typical Seyfert 1 parameters. For NGC 7469, we have chosen a black hole mass of $M_7 \equiv (M/10^7\,{\rm M}_\odot) = 1$. This is consistent with the upper range of the mass estimates by Collier et al. (1998) using broad emission line reverberation mapping. As we discussed in Paper I, the disk inner truncation radius will be largely constrained by the shape and magnitude of the optical/UV continuum. For NGC 7469, the optical and UV fluxes show evidence for the roll-over associated with the peak of the black body spectrum at this inner radius. Since the temperature distribution of the disk will nearly follow a $T_{\rm disk} \propto r^{-3/4}$ radial dependence whether the local disk flux is due to viscous dissipation or thermal reprocessing from an extended central X-ray source (see Paper I), we can use the optical and UV colors and magnitudes for NGC 7469 to estimate values for the disk inner radius $r_{\rm min}$ and the disk temperature $T_{\rm disk,max}$ at that radius. Insofar as the radial temperature distribution obtained from our more detailed thermal reprocessing plus viscous dissipation calculation does obey a $r^{-3/4}$ dependence, the values we find for $r_{\rm min}$ and $T_{\rm disk,max}$ will depend *only* on the optical and UV fluxes. Performing these fits over the 30 epochs of optical/UV data for NGC 7469, the average values we obtain are $r_{\rm min} = 3.0\pm0.3\times10^{14}$ cm and $T_{\rm disk,max} = 3.5\pm0.2\times10^4$ K. As we showed in Paper I, disk spectra computed for values of $r_{\rm min}$ which differ significantly from the above will have very different optical/UV colors if normalized to the longest wavelength optical flux. As *a posteriori* confirmation of setting $r_{\rm min} = 3\times10^{14}$ cm for NGC 7469, we note the quality of the fits to the optical/UV data shown in Fig. A7 and that the temperature distributions for those calculations do indeed have close to a $r^{-3/4}$ dependence. Now, since $r_{\rm min} \gtrsim 200 r_g$, the amount of disk emission due to viscous dissipation is insensitive to the term containing r_l in Eq. 4 and depends almost entirely on the product $M\dot{M}$. Therefore, the full range of black hole masses, $M \sim 10^6$–$10^7\,{\rm M}_\odot$, found by Collier et al. can be accommodated by adjusting $\dot{M}$ accordingly.

Simultaneous *ASCA* measurements of the broad Fe Kα line emission in NGC 3516 indicate that much of this emission originates from disk radii $\lesssim 6r_g$, very close to the central black hole (Nandra et al. 1999). Therefore we adopt a disk inner radius of $r_{\rm min} = 6r_g$, so that the choice of black hole mass also sets the value of $r_{\rm min}$. Unlike NGC 7469, the optical and UV

continuum fluxes we have for NGC 3516 do not show a high frequency roll-over, and we can infer only an upper limit for the disk truncation radius from these data. After de-reddening the optical and UV fluxes, a disk inner truncation radius of $r_{\rm min} \lesssim 1 \times 10^{13}$ cm seems to be required, yielding a black hole mass of $M \lesssim 10^7\,{\rm M}_\odot$.[3] However, a mass this small yields somewhat large values for the temperature of the Comptonizing plasma during some epochs (see Fig. A3), so we have computed models for several black hole masses $M_7 = 1$, 2, and 3.

Given values for $r_{\rm min}$ and M, several considerations limit the plausible range of accretion rates. First, since they are assumed to be constant, they must be sufficiently small to allow the observed optical and UV variability to be due to disk thermal reprocessing. Second, since the amount of disk flux and the ratio $r_s/r_{\rm min}$ determine the X-ray luminosity through the observed photon index and amplification factor scaling relation, larger accretion rates correspond to smaller thermal Comptonization roll-over energies, $E_c = 2k_BT$. The values of E_c cannot be too small, otherwise the roll-over would be evident in the observed X-ray spectra. Therefore, somewhat arbitrarily, we selected accretion rates which ensured that $k_BT \gtrsim 50$ keV in all epochs. As it turns out, this condition is more stringent than the constraint that the varying part of the optical/UV flux need be due to thermal reprocessing. On the other hand, the accretion rate must be sufficiently large so that energy balance is satisfied such that $L_{\rm untr} \gtrsim L_x + L_{\rm disk}$. Furthermore, larger accretion rates are preferred since they imply values of k_BT which are not too large. This is essential since we do not consider the effects of pair balance or emission from non-thermal particle distributions, and thus this model tacitly assumes $k_BT \lesssim m_ec^2$. The various parameters which are held constant are summarized in Tables A2 and A3.

4. RESULTS

4.1. *NGC 3516*

The model parameters and resulting light curves for NGC 3516 are shown in Fig. A3. For the $M_7 = 2$ and $M_7 = 3$ cases, the fitted plasma temperatures and optical depths are well within the range of values which have been typically measured or assumed for type 1 Seyfert galaxies (Zdziarski, Poutanen, & Johnson 2000). However, for the $M_7 = 1$ case, the plasma temperature is somewhat high in two epochs, $k_BT \sim 1$ keV. In all three cases, the size parameter of the Comptonizing region, r_s, is about a factor of 3–4 smaller than the disk inner truncation radius so that the shape of the region containing the hot plasma is relatively flat. By comparison, the range of spherical radii we found for the fits presented in Paper I were only somewhat smaller than the truncation radius, $r_s \sim 0.7\,r_{\rm min}$. The reason for this less pronounced difference can be seen in Fig. A2 in which the L_s/L_x curve for the ZLS calculation declines more rapidly as $r_s/r_{\rm min}$ decreases for $r_s/r_{\rm min} < 1$ than it does for the hybrid sphere/ellipsoid model. In the lower right panel of Fig. A3, we see that the thermal Comptonization luminosities, L_x, are consistently less than the available accretion power, $L_{\rm untr} - L_{\rm disk}$ (see Table A2). For the black hole masses and accretion rates we consider, the thermal Comptonization luminosity constitutes a substantial fraction of $L_{\rm untr} - L_{\rm disk}$, implying fairly efficient accretion, comparable to that for an untruncated thin disk in a Kerr metric.

The spectral energy distributions for these fits are shown in Fig. A4. The optical and X-ray spectra are reasonably well described by the model SEDs, but the continuum flux at 1360Å is problematic. When the reddening correction is applied, this datum sits above a $\nu F_\nu \propto \nu^{4/3}$ extrapolation from the optical data. Even if we made the model disk spectra bluer by, for example, decreasing the inner truncation radius below $r_{\rm min} = 8.9 \times 10^{12}$ cm, the 1360Å flux would still exceed the model value by $\sim 20\%$. Edelson et al. (2000) estimate systematic changes in the UV flux of 1.5% due to thermal variations, but this is too small to account for the potential discrepancy. Furthermore, given the lack of a strong X-ray flare either during or preceding the UV measurements (see Fig. 1, Edelson et al. 2000) and the $\pm 1.5\%$ relative variations in the optical light curves, which directly followed them, it is unlikely that there was a sufficiently strong flare in the disk emission to account for such a large UV continuum flux. However, the 1360Å continuum may be contaminated by the broad wings of the Si IV 1397Å and C II 1335Å emission lines. It would be extremely useful for a more complete analysis of these data to be performed that is similar to the spectral fitting by Kriss et al. (2000) for the *HST/Faint Object Spectrograph* and *IUE* spectra of NGC 7469 in order to determine the separate continuum and emission line fluxes as precisely as possible.

4.2. *NGC 7469*

The corresponding fits for NGC 7469 shown in Fig. A5 (solid diamonds) present a different picture for the inner regions of this object and seem to require additional elements in the model. First of all, the generally softer X-ray spectra imply values of r_s which are close to the disk inner radius so that the central plasma region is spherical, save for one epoch when the X-ray spectrum is its hardest. Of course, the specific values we fit for r_s also depend on our choice of $\dot{M}$. Second, the variations in the observed optical fluxes are noticeably smaller than that of the model. Part of the excess variability in the model optical light curves is due to the fact that light travel time effects are not included in these calculations. The measured time lags of ~ 1 day imply that the model curves should be smeared out on at least this time scale. However, even if such light travel time effects are included, there will still be excess variability at the ~ 10 day time scale. Nonetheless, given the simplicity of this model, it is encouraging that the shape and magnitude of the UV light curve can be so well reproduced while the relative magnitude of the optical fluxes are approximately matched and the optical variability is not greatly over-predicted.

Unfortunately, the relatively large variations in the UV flux seem to require much larger changes in the X-ray luminosity than are found by simply extrapolating the 2–10 keV flux over even as broad a range as 0.1 to 100 keV (see Nandra et al. 2000). Given the measured 2–10 keV fluxes and photon indices, the size of the L_x variations which are required by thermal reprocessing can only be accommodated by setting the thermal roll-over energy to unrealistically large values — in several epochs, we find $k_BT \gtrsim 10^5$ keV. Clearly, such large temperatures are not consistent with the underlying assumptions of these calculations. Not only would pair-production and non-thermal emission likely be present at these temperatures (Coppi 1999), the shape of the thermal Comptonization continuum at 2–10 keV would not resemble a power-law as individual scattering orders would become apparent in these spectra for temperatures $\gtrsim 10^3$ keV (e.g., Stern et al. 1995).

[3] In Paper I, the effects of reddening were not considered, and a truncation radius of $r_{\rm min} \simeq 3 \times 10^{13}$ cm was sufficient.

One way of narrowing the required temperature range is by giving the observed X-ray continuum more "leverage" in producing a greater amount of variability in the thermal reprocessed disk emission. This can be accomplished by allowing for anisotropy in the thermal Compton emission so that the X-ray intensity that we see directly is less than the X-ray intensity incident upon the accretion disk. Such anisotropy may arise in several different ways. The strong gravitational field of the central black hole will cause radiation produced near it to follow curved geodesics which may intercept the disk rather than follow straight-line trajectories to infinity (e.g., Cunningham 1975). Bulk relativistic motion of the Comptonizing plasma will beam the radiation along the direction of motion (Beloborodov 1999). However, in this case, the bulk motion would have to be directed towards the disk instead of away from it as would occur in a mildly relativistic jet. Finally, since the region of Comptonizing plasma is not being illuminated uniformly, but rather by the seed photons from the disk encircling its equator, there is a strong preference for the thermal Compton photons of the first scattering order to be directed back towards the disk.

Ideally, we would have full descriptions of the geodesics followed by the thermal Compton radiation in order to account for the aforementioned effects properly, but the use of a simple parameterization will serve to illustrate how large a difference some mild anisotropy can make. Therefore, rather than modeling the various effects in detail, we instead introduce a parameter, ξ, which describes the anisotropy so that the total luminosity of the Comptonizing plasma and the luminosity used to compute the thermal reprocessed emission is given by

$$L_x = \xi L_{x,\rm app}. \tag{17}$$

Here $L_{x,\rm app}$ is the apparent luminosity inferred from the assumed thermal roll-over, $E_c = 2k_BT$, the measured spectral index, and the measured 2–10 keV flux, i.e., it is the L_x given by Eqs. 12 and 13. Setting $\xi = 1.5$, we have recomputed the spectral fits to the NGC 7469 data and plotted the results in Fig. A5 (plus-signs). As expected, a narrower range of plasma temperatures are found which reproduce the optical/UV variability, but the plasma temperatures nonetheless reach values $k_BT \sim 10^4$ keV, which are still too large to be self-consistent.

We now ease some of the restrictions on the parameters of the X-ray spectrum. For all previous fits, we have used the best-fit values of the photon indices obtained from the X-ray spectral fitting. Since many of the spectral indices for the NGC 7469 observations are near $\Gamma \approx 2$ (see Fig. A6), a given change in the thermal roll-over energy E_c has less impact on the overall X-ray luminosity than it would for a harder spectrum with, say, $\Gamma \approx 1.6$. Therefore, in order to increase the accessible range of the X-ray luminosities, we allow the X-ray spectral index to vary within the 1-sigma bounds of the best-fit values, and we allow for small variations in the 2–10 keV flux used to compute L_x (Eq. 12). Furthermore, we restrict the plasma temperature to be 40 keV $< k_BT <$ 700 keV; and we set the anisotropy parameter to be $\xi = 1.5$, as before. With these additional conditions, we obtain the spectral fits shown in Fig. A6. For some epochs, the X-ray spectral indices attain values which are right at the 1-sigma limits, and small deviations from the observed X-ray fluxes and somewhat larger deviations in UV fluxes are now present, but the overall fits of the spectral energy distributions are largely satisfactory while maintaining a consistent range of plasma temperatures. We plot in Fig. A7, the SEDs for six exemplary epochs of the NGC 7469 data for the three cases we have considered. The details of these three fitting schemes are given in Table A3.

5. DISCUSSION AND CONCLUSIONS

Given the parameters from the above spectral fits, NGC 3516 and NGC 7469 provide contrasting cases for the characteristics of the accretion flow in the inner regions of Seyfert galaxies. NGC 3516 has a high accretion efficiency ($\gtrsim 30\%$), a small disk inner truncation radius, and a flattened, disk-like distribution of Comptonizing plasma. On the other hand, NGC 7469 has a substantially lower accretion efficiency (~ 2–3%), a large truncation radius, and a vertically extended hot plasma region. As we have noted above, the small truncation radius for NGC 3516 is consistent with the relativistically broadened iron Kα line measured by *ASCA* over the same observing period. Although similar *ASCA* observations were not taken during the 1996 campaign for NGC 7469, Nandra et al. (2000) found iron Kα equivalent widths of ~ 150 eV from the *RXTE/PCA* data. This value agrees with the equivalent width measured during the November 1993 *ASCA* observations by Guainazzi et al. (1994) who found the iron Kα emission line to be very narrow. If the Fe Kα line is composed of emission from a disk, then Guainazzi et al. concluded that it must originate at least several tens of Schwarzschild radii from the central black hole, consistent with our estimate for the disk inner truncation radius of $r_{\rm min} \simeq 200 r_g$.

As we discussed in the Introduction, a similar analysis was performed by Poutanen et al. (1997) for the X-ray binary Cygnus X-1. With respect to the semi-analytic model they used, the main difference between that work and the present is in the empirical relation employed by those authors to characterize the thermal Comptonization spectrum in terms of the model parameters. In particular, rather than Eq. 15, Poutanen et al. used the scaling relation

$$\Gamma = \left(\frac{20}{3A}\right)^{1/4} + 1 \tag{18}$$

which was found from Comptonization modeling by Pietrini & Krolik (1995).[4] On the observational side, since Cygnus X-1 is significantly brighter in the hard X-rays than any Seyfert galaxy, both the roll-over energy of the thermal Comptonization continuum and the amplitude of the Compton reflection component for Cygnus X-1 could be measured directly. These data provided Poutanen et al. with estimates of the plasma temperature as well as the ratio $r_s/r_{\rm min}$. In addition, the thermal disk spectrum, which was observable in the soft X-rays, gave them constraints on the accretion disk flux and the inner disk radius. Armed with this information, Poutanen et al. were able to apply the scaling relation and the assumed sphere+disk geometry to determine the mass accretion rate directly in both the hard and soft spectral states rather than to have to assume values for the accretion rates based on "reasonable" ranges for parameters such as the plasma temperature, as we have done here.

As the analysis of the Cygnus X-1 data demonstrates, more stringent tests of this model in its application to Seyfert galaxies will be available when the hard X-ray/soft gamma-ray spectra from these objects can be reliably measured on sufficiently short time scales to detect the changes in the spectral roll-over implied by the temperature curves in Figs. A3, A5, and A6. This will require a hard X-ray telescope with a large effective area at these energies such as that proposed for *ASTRO-*

[4] Eq. 18 differs numerically from the expression used by ZLS, Eq. 1, by only $\lesssim 3\%$ for photon indices ranging from $\Gamma = 1.4$ to 2.3.

E2. Nonetheless, relevant constraints for the mean properties of the Comptonizing plasma may be ascertained from existing longer time scale observations by the *Beppo-SAX* satellite and the *Oriented Scintillation Spectrometer Experiment (OSSE)* aboard the *Compton Observatory* and from forthcoming observations which will be available with *INTEGRAL*. For example, spectral fits of data from *OSSE* observations of NGC 4151 (Johnson et al. 1997) and from *Beppo-SAX* observations of NGC 5548 (Nicastro et al. 2000) suggest that as the X-ray power-law spectrum softens, the cut-off energy (or equivalently, the plasma temperature) increases, contrary to naive expectations from thermal Comptonization models. However, since the Thomson depth of the plasma may also change simultaneously, a sufficiently large decrease may more than compensate for any spectral hardening which a temperature increase would otherwise imply. In Fig. A8, we plot the plasma temperatures versus the measured X-ray spectral indices for the "optimal" case fits of the NGC 7469 data (i.e., $\xi = 1.5$ and Γ allowed to vary) and for the three cases we considered for NGC 3516. It is clear that a strict relationship between k_BT and Γ is not required. Since changes in k_BT will affect both L_x and the thermal reprocessing contribution to the disk emission, simultaneous optical and UV monitoring will be necessary in order for longer term measurements of the hard X-ray spectra of Seyfert 1s to constrain thermal Comptonization models in which thermal reprocessing plays an important role.

Greater spectral coverage in the hard X-ray band will also provide improved constraints on the apparent correlation between the thermal Comptonization spectral index and the relative strength of the Compton reflection component. However, the predictions of the ZLS analysis are altered since the inclusion of disk emission due to viscous dissipation implies quite different estimates for the seed photon luminosities. The X-ray spectral indices will no longer be solely a function of the geometry, and simultaneous optical and UV monitoring along with broad band X-ray spectroscopy will again be necessary to determine the strength of the Compton reflection component implied by this model.

In fact, for the present data, we do find significant differences between the predicted reflection fractions and the values obtained by fitting the PEXRAV model to the *RXTE/PCA* data. In addition, the reflection fraction given by this model for a specific viewing angle can differ substantially from the *average* Compton reflection strength as defined by ZLS. Following ZLS, the total thermal Comptonization luminosity intercepted by the disk is

$$L_d = 4\pi \int_{r_{\rm min}}^{\infty} dr\, r F_{\rm inc}(r), \tag{19}$$

where the incident flux $F_{\rm inc}$ is given by Eqs. 2 or 7. This is the luminosity intercepted by *both* sides of the disk. ZLS define the reflection fraction, averaged over all viewing angles, to be the ratio of the luminosity intercepted by the disk and the thermal Comptonization luminosity which can be seen by distant observers:

$$R_{\rm ZLS} = \frac{L_d}{L_x - L_d}. \tag{20}$$

When comparing the observed R-Γ correlation for a large sample of objects which have random orientations, this is the appropriate form to use for the reflection fraction. However, for a specific object with a known inclination, this expression may not be a good approximation. In particular, for an object with disk inclination $i = 0$ and plasma radius $r_s \leq r_{\rm min}$, the full X-ray luminosity from the Comptonizing plasma is seen, but only half of the disk reprocessing emission is observed. In this case, one should use

$$R_{i=0} = \frac{L_d/2}{L_{x,\rm app}}. \tag{21}$$

Note that the apparent X-ray luminosity appears in the denominator, but L_d in the numerator is computed using $L_x = \xi L_{x,\rm app}$ to account for any anisotropy. In Fig. A9, we plot the R-Γ relationships using these two expressions for the reflection fraction along with the fitted values from our analysis of the *RXTE/PCA* data for NGC 3516 and from the analysis of Nandra et al. (2000) for NGC 7469. The model values using $R_{i=0}$ clearly under-predict the fitted values by a substantial amount and are also much smaller than the average values, $R_{\rm ZLS}$. As Nandra et al. (2000) point out, any apparent correlation between spectral index and Compton reflection strength may be partially due to a statistical correlation between the parameters which arise from model fitting rather than from intrinsic properties of the source. The presence of such a statistical correlation between fitting parameters suggests that the small reflection fractions given by this model may be accommodated by the data if the underlying thermal Comptonization spectra are actually somewhat harder than those found by fitting the simple reflection models to the *RXTE/PCA* data. Since *RXTE* observations generally do not provide much useful spectral coverage above ~ 15 keV for Seyfert galaxies, more sensitive hard X-ray continuum measurements for energies $\gtrsim 10$ keV are required to resolve this discrepancy.

Even in the absence of high quality hard X-ray data to measure the thermal roll-over or the Compton reflection fraction definitively, certain aspects of this model are indeed tested by the available data, though the constraints are not as direct. For example, if the UV fluxes for NGC 7469 were consistent with an extrapolation of the $\nu F_\nu \sim \nu^{4/3}$ dependence of the optical data, then a much smaller disk inner truncation radius would be required. This in turn would imply a much broader Fe Kα emission line that may contradict the observations of a narrow line by Guainazzi et al. (1994), or it may require a much smaller black hole mass, which could be in conflict with the reverberation mapping estimates of Collier et al. (1998). Furthermore, the quantity $M\dot{M} \sim 10^6\ {\rm M_\odot}^2\ {\rm yr}^{-1}$ which we find for NGC 7469 (see Table A3) is in rough accord with the value of $M\dot{M} \simeq 0.7 \times 10^6\ {\rm M_\odot}^2\ {\rm yr}^{-1}$ found by Collier et al. (1998) by fitting interband continuum lags for these same observations.

The large disk inner truncation radius and vertically extended Comptonizing region we find for NGC 7469 suggests that the inner regions of this object may consist of an advection dominated accretion flow (ADAF) similar to those which have been used to model the X-ray spectra of Galactic X-ray binaries (e.g., Esin, McClintock, & Narayan 1997; Esin et al. 2001). However, the mass accretion rate which we find for NGC 7469 in our optimal case, $\dot{M} \simeq 0.15\,{\rm M_\odot\ yr^{-1}}$, is larger than the Eddington limit by a factor of ~ 3, assuming a Kerr metric and a $10^7\,{\rm M_\odot}$ black hole; and it is $\sim 40\%$ of the Eddington limit for a standard thin disk in a Schwarzschild metric. This accretion rate likely exceeds the critical accretion rate found by Narayan & Yi (1995) of $\dot{M}_{\rm crit} \sim \alpha^2 \dot{M}_{\rm Edd}$, below which advection dominated flow is expected to occur. The anomalous viscosity parameter is found in magnetohydrodynamic simulations of disks to have values $\alpha \lesssim 0.1$ (e.g., Balbus & Hawley 1998). As we noted above, we chose the largest possible accretion rates for our models which were consistent with a minimum plasma

temperature of $k_B T \simeq 50$ keV and with the variations in the optical and UV light curves being due to thermal reprocessing. We could have chosen smaller values of the accretion rates in order to satisfy the limits imposed by $\dot{M}_{\rm crit}$, but that would necessitate increasing the plasma temperatures in order to have larger thermal Comptonization luminosities, possibly violating our implicit constraint of $kT \lesssim m_e c^2$ for NGC 3516 and worsening the situation for NGC 7469. Furthermore, the lower accretion rates would require much greater radiative efficiencies, and for NGC 3516, the efficiency is already a fair fraction of unity. We could trade off reductions in the intrinsic disk luminosity with a larger anisotropy factor, but values of $\xi \gg 1$ would likely be required.

However, for NGC 7469, our analysis really has only constrained the quantity $M\dot{M} \simeq 1.5 \times 10^6$ $M_\odot{}^2$ yr^{-1}. If the central black hole mass were $M \simeq 10^8$ $M_\odot$, then we would have $\dot{M} \simeq 0.03 \dot{M}_{\rm Edd}$ which would just satisfy the accretion rate limit for advection for $\alpha \sim 0.2$, assuming a Kerr metric. Since the reverberation mapping estimates of the black hole mass in NGC 7469 are given by $M \propto R_{\rm BLR} v_{\rm BLR}^2 / G$, where $R_{\rm BLR}$ and $v_{\rm BLR}$ are (model-dependent) length and velocity scales which characterize the broad line region, these quantities would have to be each underestimated by factors of $\sim 10^{1/3} \sim 2$ in order to account for an order-of-magnitude discrepancy in the central black hole mass (see Peterson & Wandel 2000). For a Schwarzschild metric, a central black hole mass of $M \simeq 3 \times 10^7$ $M_\odot$would yield an accretion rate $\dot{M} \sim 0.04 \dot{M}_{\rm Edd}$. In this case, $R_{\rm BLR}$ and $v_{\rm BLR}$ would need only each be underestimated by a factor ~ 1.4. For $M = 3 \times 10^7$ $M_\odot$, we have $r_{\rm min}/r_g \sim 60$ which would still be consistent with the *inferred* appearance of a narrow Fe Kα line in the *RXTE/PCA* spectra.

By contrast, the required accretion rate for NGC 3516, assuming $M = 2 \times 10^7 M_\odot$ and a Kerr metric, is $\dot{M} \sim 0.09 \dot{M}_{\rm Edd}$. This too nominally exceeds $\dot{M}_{\rm crit}$; and since we have assumed $r_{\rm min} = 6 r_g$, there is not much freedom here to increase the central black hole mass in order to increase $\dot{M}_{\rm Edd}$ and decrease $\dot{M}$. If we assume $r_{\rm min} = 2 r_g$, which is still consistent with the Fe Kα emission line fits of Nandra et al. (1999), the black hole mass could be larger by a factor ~ 3, and we would have $\dot{M} \sim 0.03 \dot{M}_{\rm Edd}$. In any case, since the inner hot accretion flow we infer from our model is more "disk-like" than that of NGC 7469, a larger accretion rate relative to $\dot{M}_{\rm Edd}$ for NGC 3516 may nonetheless be consistent in some sense with the "strong ADAF proposal" of Narayan & Yi (1995; see also Narayan, Mahadevan, & Quataert 1998), which states that NGC 3516 should then be less likely to have an ADAF-like flow than NGC 7469. Clearly, these machinations illustrate the speculative nature and uncertainties involved in extracting physical significance from our simple spectral fits based on the radiative processes. Regardless, the more plausible of the above suggestions are not wildly out of line with the observations or theoretical expectations. This perhaps indicates that this sort of modeling is on the cusp of actually providing useful constraints on the dynamical models.

Numerous physical considerations which have not been included in these calculations may affect our results. In the case of a flattened Comptonizing region, such as we found for NGC 3516, the mean Thomson depth through the plasma will vary significantly depending on the scattering order. Along with the non-uniform illumination of the Comptonizing region by the disk photons, this would lead us to expect to see features in the X-ray spectrum similar to the anisotropy breaks found by Stern et al. (1995) in their thermal Comptonization models of disk coronae. If the Comptonizing regions are threaded by sufficiently strong magnetic fields, then thermal synchrotron radiation can make a large contribution to the seed photon flux and thus reduce the importance of the disk radiation in determining the energy balance of the plasma as in the ADAF model of Esin et al. (2001). However, Wardziński & Zdziarski (2000) have argued that for Seyfert 1s the disk thermal emission should be a much more important source of seed photons than thermal synchrotron emission except for very low luminosity sources which have $L/L_{\rm Edd} \lesssim 10^{-4}$. Finally, as we have already discussed, enhanced illumination of the disk due to photons following curved geodesics or anisotropy in the scattered radiation will clearly alter both the thermally reprocessed disk flux as well as the Compton reflection strength.

Despite these deficiencies, the relative success of this model in reproducing the optical, UV and X-ray flux and spectral variability observed from NGC 3516 and NGC 7469 underscores the crucial point that *any* model which attempts to describe the emission in these objects must at least take into account the roles that feedback and energy balance play in determining the emission across a wide range of energies. As corollary to this, observations of these objects would do well to consist of simultaneous broad band spectral coverage, from the optical to the soft gamma-rays, in order to maximize the constraints on this and future, more sophisticated radiative and dynamical models.

The author would like to thank the anonymous referee for very helpful comments which have greatly improved this paper, Omer Blaes for many useful discussions, and Mike Nowak for helpful comments on the manuscript. This work was partially supported by NASA ATP grant NAG 5-7723. This research has made use of data obtained from the High Energy Astrophysics Science Archive Research Center (HEASARC), provided by NASA's Goddard Space Flight Center; and it has also made use of the NASA/IPAC Extragalactic Database (NED) which is operated by the Jet Propulsion Laboratory, California Institute of Technology, under contract with NASA.

APPENDIX

FORMULAE FOR COMPUTING DISK INCIDENT FLUXES AND SEED PHOTON LUMINOSITIES

Deriving these formulae from the specified geometry is straight-forward. We present the following expressions for completeness. Here all lengths are in units of $r_{\rm min}$, i.e., $\tilde{r} = r/r_{\rm min}$, etc..

$\tilde{r}_s \geq 1$ (Spherical case, same as ZLS):

$$\alpha_{\rm max} = \pi/2, \qquad \tilde{r} \leq \tilde{r}_s, \tag{A1}$$

$$= \sin^{-1}(\tilde{r}_s/\tilde{r}), \qquad \tilde{r} > \tilde{r}_s, \tag{A2}$$

$$\phi_{\rm max} = \pi, \qquad \tilde{r} \leq \tilde{r}_s, \tag{A3}$$

$$= \cos^{-1}\left[\frac{(\tilde{r}^2 - \tilde{r}_s^2)^{1/2}}{\tilde{r}\cos\alpha}\right], \qquad \tilde{r} > \tilde{r}_s, \tag{A4}$$

$$\tilde{l} = \cos\alpha(\tilde{r}\cos\phi + [\tilde{r}_s^2(1+\tan^2\alpha) - \tilde{r}^2(\sin^2\phi + \tan^2\alpha)]^{1/2}), \qquad \tilde{r} \leq \tilde{r}_s, \tag{A5}$$

$$= 2\cos\alpha[\tilde{r}_s^2(1+\tan^2\alpha) - \tilde{r}^2(\sin^2\phi + \tan^2\alpha)]^{1/2}, \qquad \tilde{r} > \tilde{r}_s. \tag{A6}$$

$\tilde{r}_s < 1$ (Ellipsoidal case):

$$\alpha_{\rm max} = \tan^{-1}\left[\frac{\tilde{r}_s}{(\tilde{r}^2 - 1)^{1/2}}\right] \tag{A7}$$

$$\phi_{\rm max} = \cos^{-1}\left[\frac{[(\tilde{r}^2 - 1)(\tilde{r}_s^2 + \tan^2\alpha)]^{1/2}}{\tilde{r}\tilde{r}_s}\right] \tag{A8}$$

$$\tilde{l} = \frac{2\tilde{r}_s[(\tilde{r}_s^2 + \tan^2\alpha) - \tilde{r}^2(\tan^2\alpha + \tilde{r}_s^2\sin^2\phi)]^{1/2}}{\cos\alpha(\tilde{r}_s^2 + \tan^2\alpha)} \tag{A9}$$

REFERENCES

Balbus, S. A., & Hawley, J. F. 1998, Rev. Mod. Phys., 70, 1
Beloborodov, A. M. 1999, in High Energy Processes in Accreting Black Holes, eds. J. Poutanen and R. Svensson, (San Francisco: Astronomical Society of the Pacific), 295
Blandford, R. D., & Begelman, M. C. 1999, MNRAS, 303, L1
Cardelli, J. A., Clayton, G. C., & Mathis, J. S. 1989, ApJ, 345, 245
Chiang, J., & Blaes, O., 2001a, ApJ, 557, L15 (Paper I)
Chiang, J., & Blaes, O., 2001b, in Proceedings of JHU/LHEA Workshop on X-ray Emission from Accretion onto Black Holes, in press
Collier, S., et al. 1998, ApJ, 500, 162
Collin-Souffrin, S. 1991, A&A, 249, 344
Coppi, P. S. 1999, in High Energy Processes in Accreting Black Holes, eds. J. Poutanen and R. Svensson, (San Francisco: Astronomical Society of the Pacific), 375
Courvoisier, T. J.-L., & Clavel, J. 1991, A&A, 248, 389
Cunningham, C. T. 1975, ApJ, 202, 788
Edelson, R. E., et al. 2000, ApJ, 534, 180
Esin, A. A., McClintock, J. E., & Narayan, R. 1997, ApJ, 489, 865
Esin, A. A., et al. 2001, ApJ, 555, 483
Guainazzi, M., Matsuoka, M., Piro, L., Mihara, T., & Yamauchi, M., 1994, ApJ, 436, L35
Haardt, F., & Maraschi, L. 1991, ApJ, 380, L51
Hubeny, I., Agol, E., Blaes, O., Krolik, J. H. 2000, ApJ, 533, 710
Hubeny, I., Blaes, O., Krolik, J. H., Agol, E. 2001, ApJ, 559, 680
Johnson, W. N., et al. 1997, ApJ, 482, 173
Krolik, J. H., et al. 1991, ApJ, 371, 541
Kriss, G. A., Peterson, B. M., Crenshaw, D. M., & Zheng, W. 2000, ApJ, 535, 58
Malzac, J., Beloborodov, A. M., & Poutanen, J. 2001, MNRAS, 326, 417
Nandra, K., et al. 1998, ApJ, 505, 594
Nandra, K., George, I. M., Mushotzky, R. F., Turner, T. J., & Yaqoob, T. 1999, ApJ, 523, L17
Nandra, K., et al. 2000, ApJ, 544, 734
Narayan, R., & Yi, I. 1995, ApJ, 452, 710
Narayan, R., Mahadevan, R., & Quataert, E. 1998, in Theory of Black Hole Accretion Disks, eds. M. A. Abramowicz, G. Bjornsson and J. E. Pringle (Cambridge University Press) 148
Narayan, R., Igumenshchev, I. V., & Abramowicz, M. A. 2000, ApJ, 539, 798
Nicastro, F., et al. 2000, ApJ, 536, 718
Peterson, B., & Wandel, A. 2000, ApJ, 540, L13
Pietrini, P., & Krolik, J. H. 1995, ApJ, 447, 526
Poutanen, J., Krolik, J. H., & Ryde, F. 1997, MNRAS, 292, L21
Quataert, E., & Gruzinov, A. 2000, ApJ, 539, 809
Schlegel, D. J., Finkbeiner, D. P., Davis, M. 1998, ApJ, 500, 525
Shapiro, S. L., Lightman, A. P., & Eardley, D. N. 1976, ApJ, 204, 187
Sincell, M. W., & Krolik, J. H. 1997, ApJ, 476, 605
Stern, B. L., Poutanen, J., Svensson, R., Sikora, M., & Begelman, M. C. 1995, ApJ, 449, L13
Wanders, I., et al. 1997, ApJS, 113, 69
Wardziński, G., & Zdziarski, A. A. 2000, MNRAS, 314, 183
Welsh, W. F., Peterson, B. M., Koratkar, A. P., & Korista, K. T. 1998, ApJ, 509, 118
Zdziarski, A. A., Poutanen, J., Mikołajewska, J., Gierliński, M., Ebisawa, K, & Johnson, W. N. 1998, MNRAS, 301, 435
Zdziarski, A. A., Lubiński, P., & Smith, D. A., 1999, MNRAS, 303, L11 (ZLS)
Zdziarski, A. A., Poutanen, J., & Johnson, W. N., 2000, ApJ, 542, 703

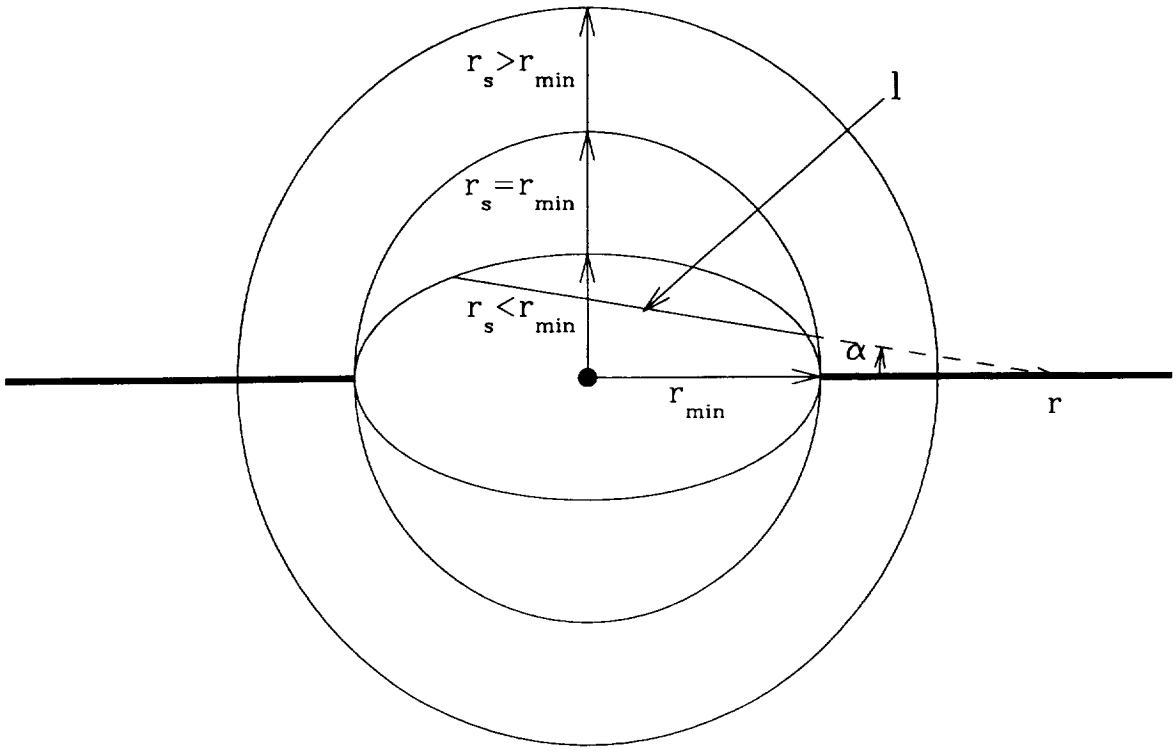

FIG. A1.— Model geometries of the Comptonizing plasma. For $r_s \geq r_{min}$, the plasma region is a sphere, and for $r_s < r_{min}$ it is an ellipsoid with semi-major axis r_{min} and semi-minor axis r_s. A sample ray is shown with a path length l through the ellipsoidal Comptonizing region and making an angle α with respect to the disk plane.

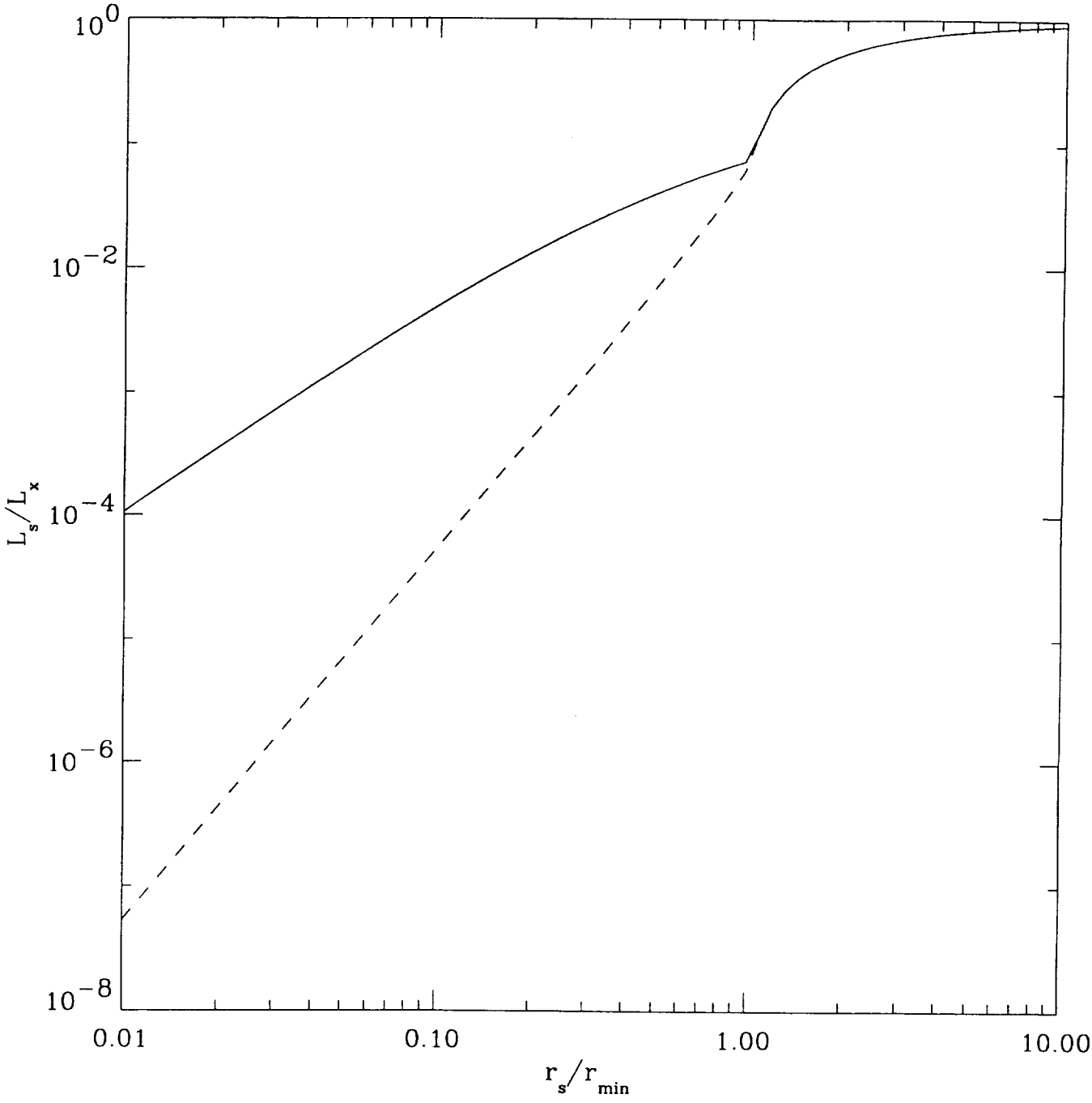

FIG. A2.— The ratio of seed photon luminosity to thermal Comptonization luminosity, L_s/L_x, versus r_s/r_{min} assuming zero contribution from viscous dissipation. The solid curve is for the hybrid sphere/ellipsoid model, and the dashed curve is for the sphere+disk model described by ZLS.

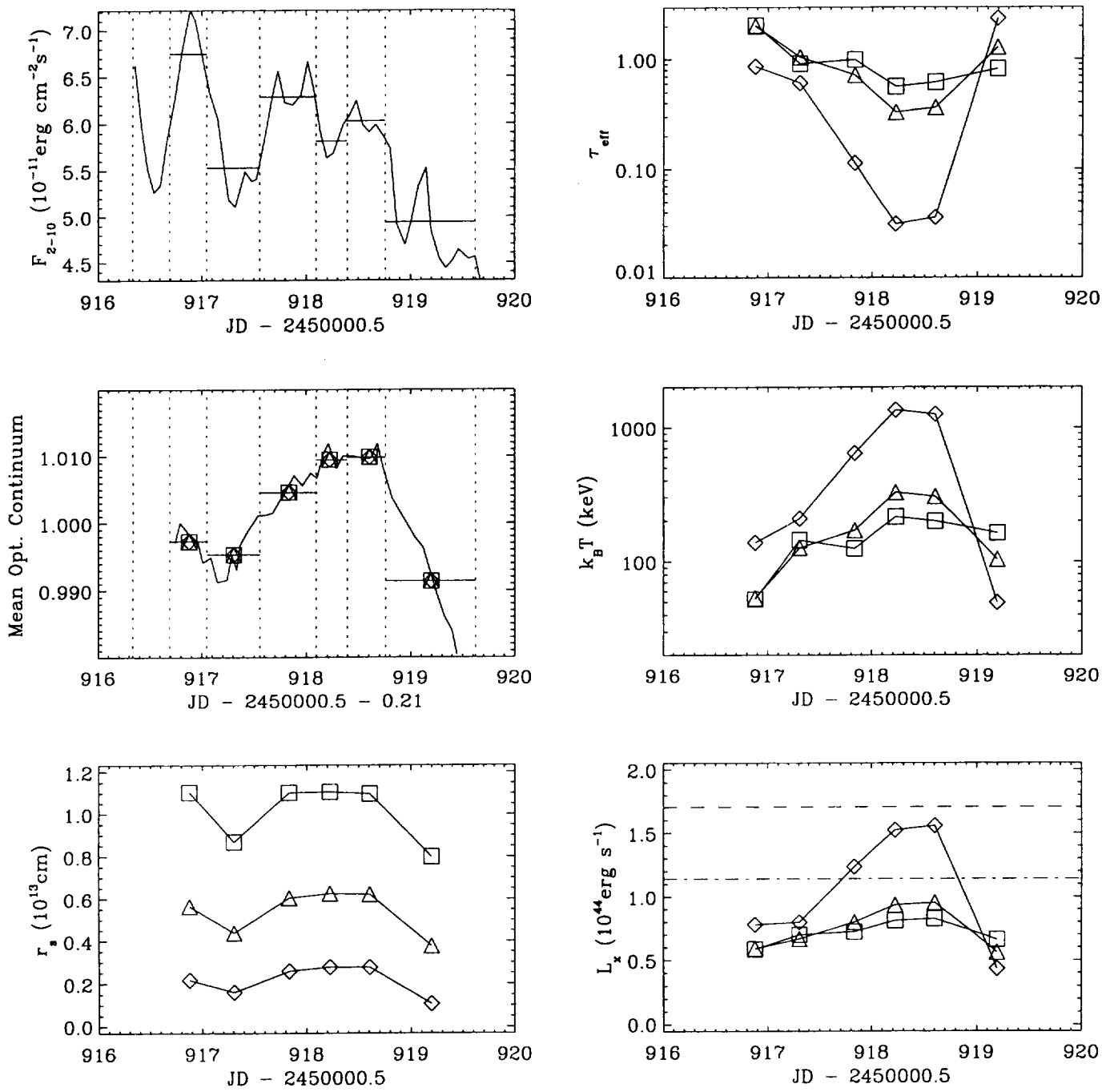

FIG. A3.— Model fluxes and fitted parameters for NGC 3516. The upper left plot shows the 2–10 keV X-ray light curve (solid curve). The dotted vertical lines are the boundaries of the epochs used to determine the X-ray spectral indices, and the horizontal line segments are the mean fluxes that were used to compute L_x (see Eqs. 12 and 13). The middle left plot shows the optical continuum light curve (solid curve) averaged over the fluxes at 3590Å, 4235Å, and 5510Å and scaled to unity. Also shown are the mean values for each epoch (line segments), and the fitted values for $M_7 = 1$ (diamonds), 2 (triangles), and 3 (squares). The lower right plot shows the thermal Comptonization luminosities compared to the available accretion power for $M_7 = 2$ (dashed line) and $M_7 = 3$ (dot-dashed line). The value for $M_7 = 1$ is $L_{untr} - L_{disk} = 3.36 \times 10^{44}$ erg s^{-1} (see Table A2).

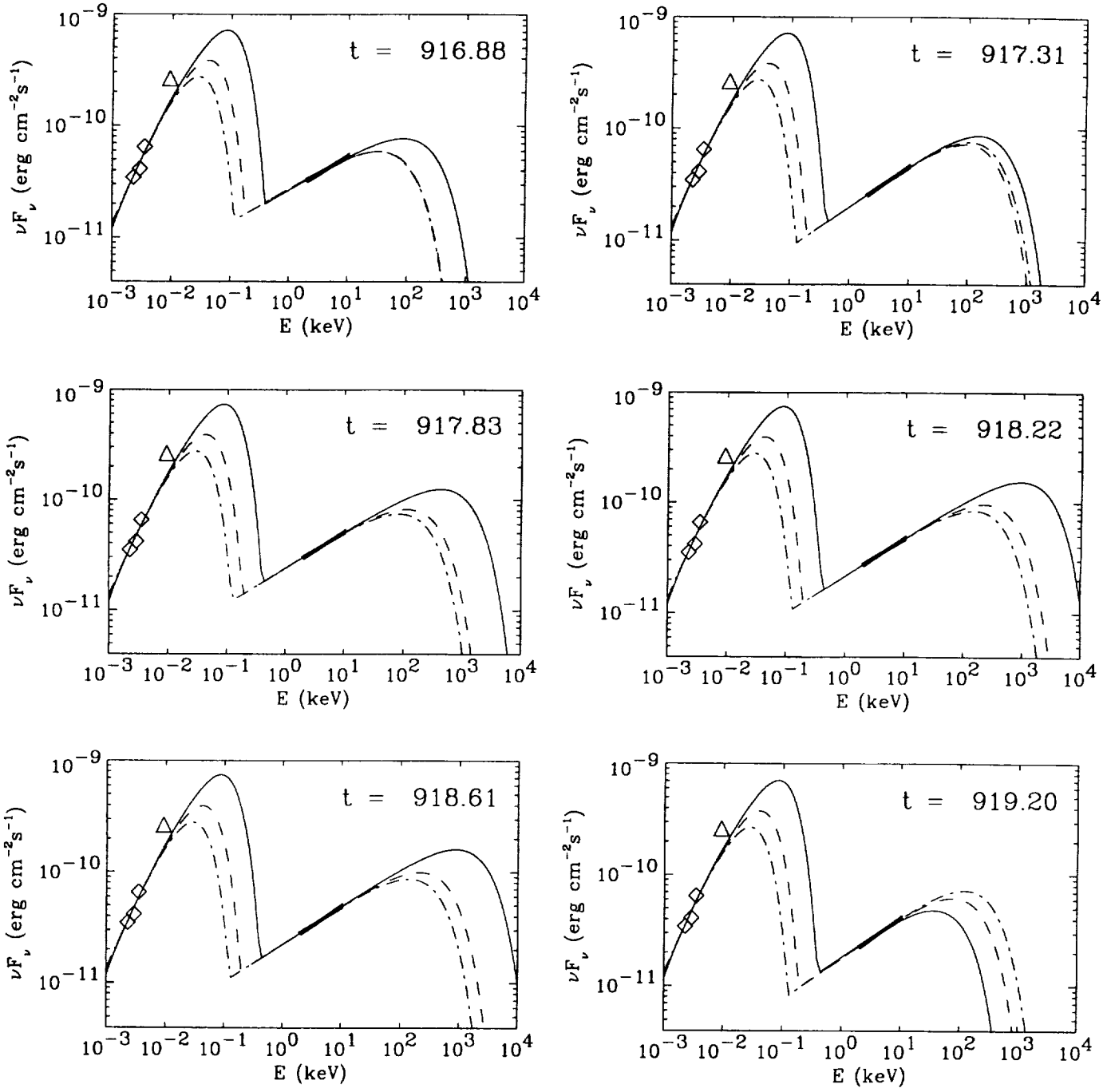

FIG. A4.— Model spectral energy distributions for NGC 3516 compared to the observed spectra. The SEDs are show for M_7 = 1 (solid curve), 2 (dashed), 3 (dot-dashed). The diamonds are the de-reddened optical fluxes from Edelson et al. (2000) which have been used in the fits to the disk thermal spectra. The triangle in each plot is the de-reddened non-simultaneous flux at 1360Å. The thick line segments are the 2–10 keV power-law continua which we have fit to the archival *RXTE* data.

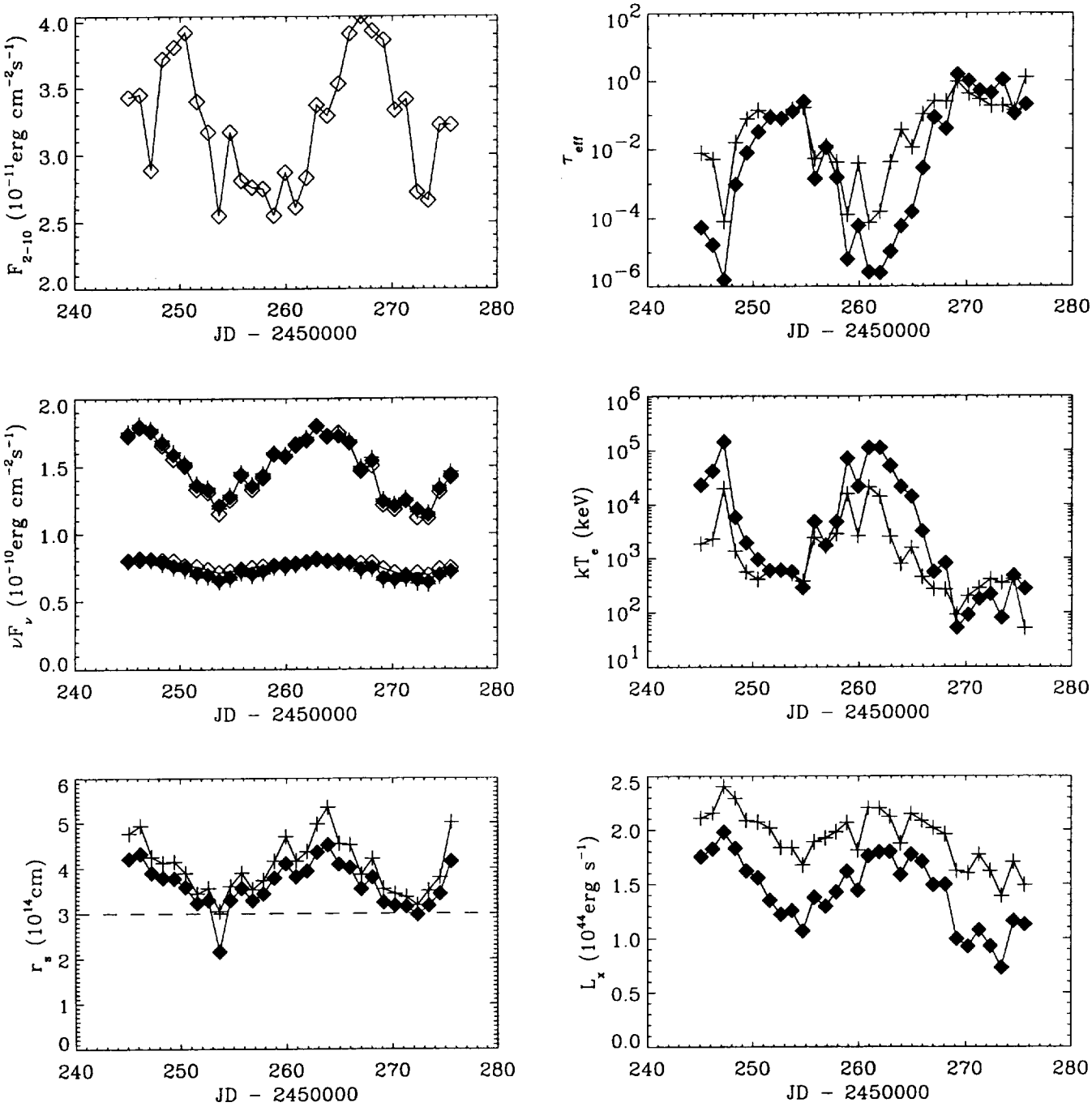

FIG. A5.— Model light curves and fitted parameters for NGC 7469 using anisotropy parameter values $\xi = 1$ (filled diamonds), corresponding to isotropic thermal Compton emission, and $\xi = 1.5$ (plus-signs); see Eq. 17. In the middle left plot, the measured fluxes are the open diamonds joined by line segments. The upper set of curves are the 1315Å fluxes, and the lower set of curves are the 4865Å fluxes. The dashed line in the lower left panel is the disk inner truncation radius, $r_{min} = 3 \times 10^{14}$ cm.

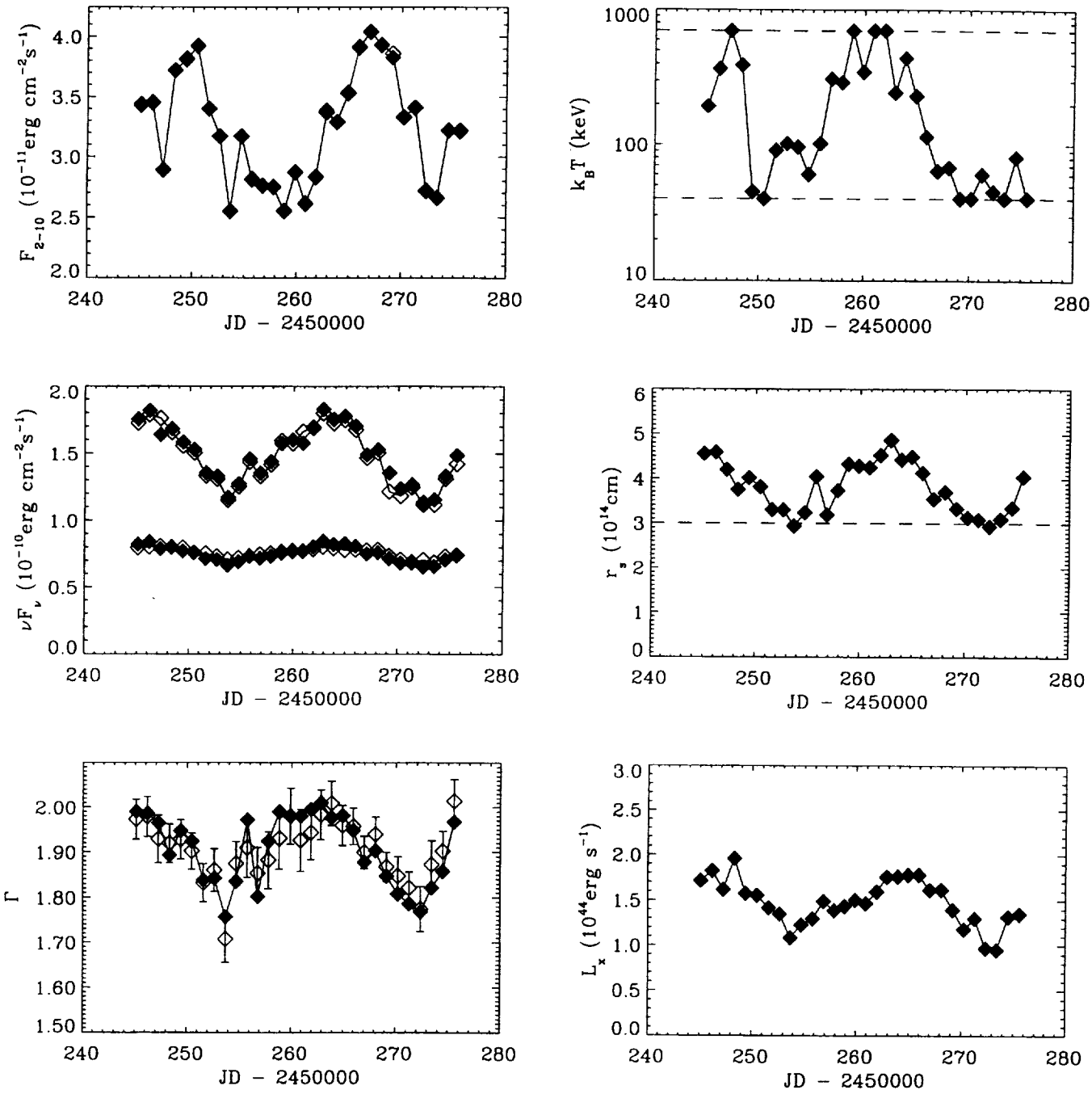

FIG. A6.— Model light curves and fitted parameters for NGC 7469 using $\xi = 1.5$ and allowing the X-ray spectral indices for each epoch to vary within the measured 1-σ bounds. The open diamonds are the measured or best-fit values determined from the data while the filled diamonds are the model values or parameters found from our spectral fits.

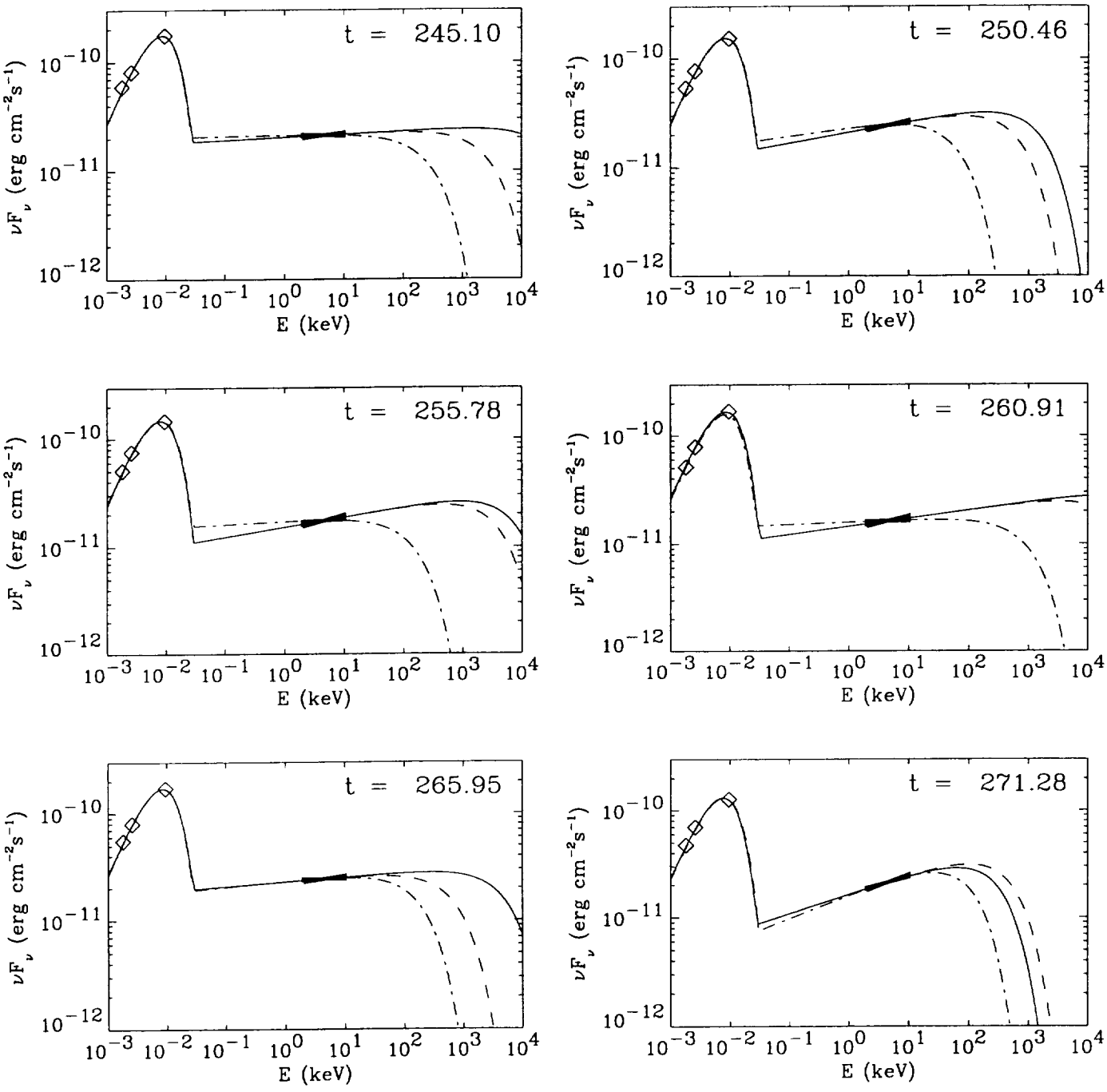

FIG. A7.— A subset of the model spectral energy distributions for NGC 7469. The solid and dashed curves correspond to ξ = 1 and ξ = 1.5, respectively, using fixed values for the X-ray spectral indices, Γ. The dot-dashed curves are the SEDs found by allowing the Γ-values to vary within the 1-σ bounds and using ξ = 1.5. The open diamonds are the starlight subtracted, de-reddened optical and UV fluxes from 1996 monitoring campaign. The thick line segments are the 2–10 keV power-law continua from the fit parameters given in Nandra et al (2000).

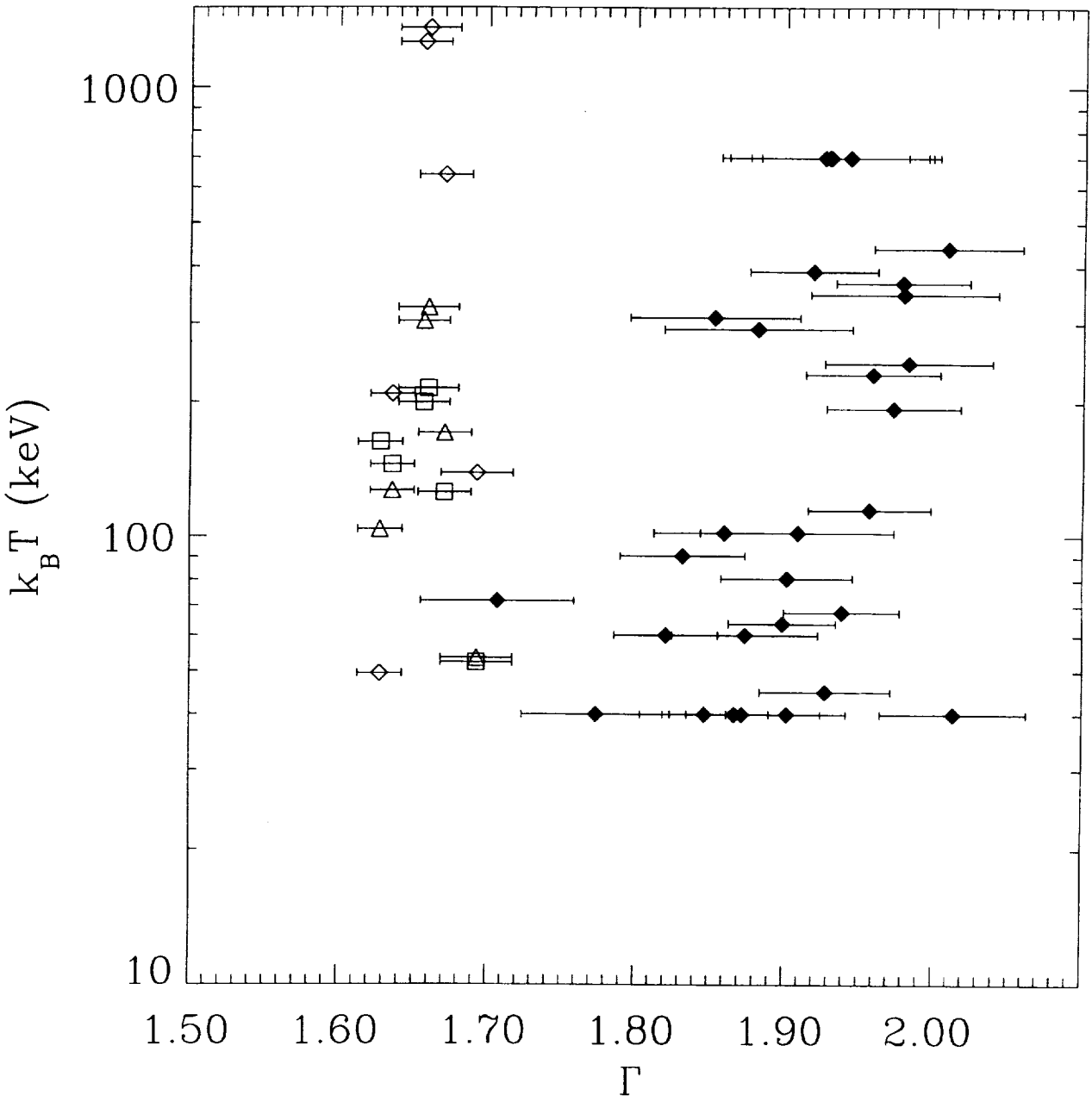

FIG. A8.— Model plasma temperatures versus measured X-ray spectral indices. The open symbols are the NGC 3516 best-fit values for M_7 = 1 (diamonds), 2 (triangles), and 3 (squares), and the filled diamonds are the values obtained for NGC 7469 using ξ = 1.5 and allowing Γ to vary.

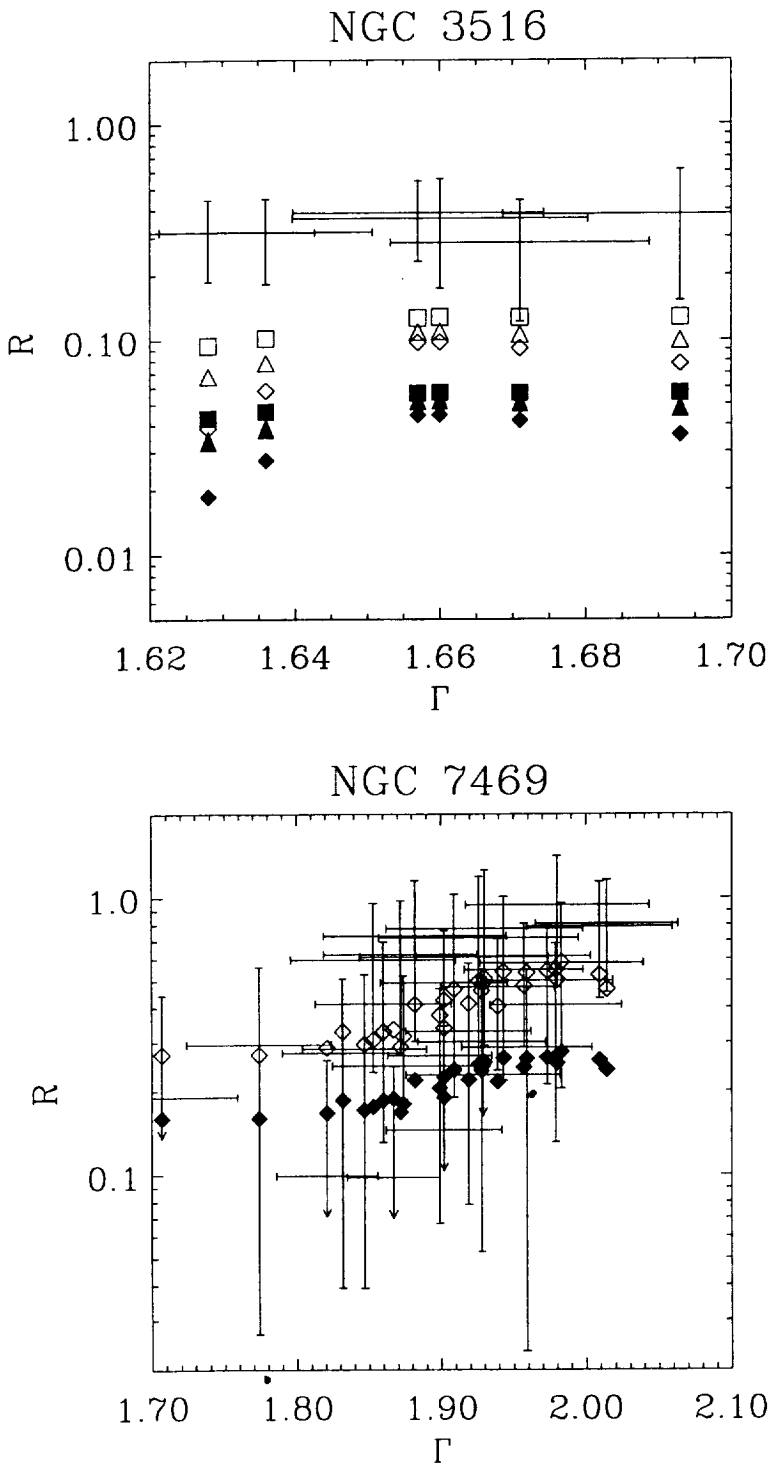

FIG. A9.— Compton reflection fraction versus X-ray spectral index for NGC 3516 (upper figure) and NGC 7469 (lower). The filled symbols are for $R_{i=0} = L_d/2L_{x,\mathrm{app}}$ which is the implied reflection fraction for a face-on geometry, while the open symbols are for $R_{\mathrm{ZLS}} = L_d/(L_x - L_d)$ which is the *mean* reflection fraction as defined by ZLS. The reflection fractions and spectral indices obtained from fitting the PEXRAV model to the *RXTE/PCA* data are shown with the error bars.

TABLE A1

OPTICAL AND X-RAY DATA FOR THE 1998 APRIL OBSERVATIONS OF NGC 3516

start time (JD - 2450000.5)	duration (ks)	F_{3590}	F_{4235}	F_{5510} (10^{-14}erg cm^{-2}s^{-1}Å^{-1})	F_{2-10} (10^{-11}erg cm^{-2}s^{-1})	Γ
916.692	30.7	1.8052	0.9536	0.6294	6.75	1.693 ± 0.024
917.048	44.2	1.8016	0.9518	0.6282	5.53	1.636 ± 0.015
917.559	46.2	1.8182	0.9606	0.6340	6.29	1.671 ± 0.018
918.094	25.9	1.8271	0.9652	0.6371	5.81	1.660 ± 0.020
918.393	31.6	1.8278	0.9656	0.6373	6.03	1.657 ± 0.017
918.759	74.6	1.7945	0.9480	0.6257	4.94	1.628 ± 0.015

TABLE A2

FIXED MODEL PARAMETERS, LUMINOSITIES, AND RADIATIVE EFFICIENCIES FOR NGC 3516

parameter	value		
$\cos i$	0.820		
d_l (10^{26} cm)	1.22		
M (10^7 M$_\odot$)	1	2	3
$r_{\rm min}$ (10^{13} cm)	0.89	1.78	2.67
$\dot{M}$ (10^{-2}M$_\odot$yr^{-1})	1.86	0.946	0.633
$L_{\rm untr}$ (10^{44} erg s^{-1})	5.26	2.67	1.79
$L_{\rm disk}$ (10^{44} erg s^{-1})	1.90	0.97	0.65
$L_{x,\rm avg}$ (10^{44} erg s^{-1})	1.05	0.75	0.72
$(L_{x,\rm avg}+L_{\rm disk})/\dot{M}c^2$	0.28	0.32	0.38
$(L_{x,\rm avg}+L_{\rm disk})/L_{\rm Edd}$	0.23	0.07	0.03

TABLE A3

FIXED MODEL PARAMETERS, LUMINOSITIES, AND RADIATIVE EFFICIENCIES FOR NGC 7469

parameter	value		
$\cos i$	0.866		
d_l (10^{26} cm)	2.06		
M (10^7 M$_\odot$)	1		
$r_{\rm min}$ (10^{13} cm)	30.		
ξ (anisotropy)	1	1.5	1.5
Γ (allowed variation)	fixed		$\pm 1\sigma$
$\dot{M}$ (M$_\odot$yr^{-1})	0.159	0.116	0.150
$L_{\rm untr}$ (10^{44} erg s^{-1})	45.0	32.8	42.5
$L_{\rm disk}$ (10^{44} erg s^{-1})	0.63	0.46	0.60
$L_{x,\rm avg}$ (10^{44} erg s^{-1})	1.43	1.93	1.47
$(L_{x,\rm avg}+L_{\rm disk})/\dot{M}c^2$	0.023	0.036	0.024
$(L_{x,\rm avg}+L_{\rm disk})/L_{\rm Edd}$	0.16	0.19	0.16